New Phytologist

Research

Bulbous perennials precisely detect the length of winter and adjust flowering dates

Imre M. Jánosi[1,2], Dániel Silhavy[3], Júlia Tamás[4] and Péter Csontos[5]

[1]Department of Physics of Complex Systems, Eötvös Loránd University, Pázmány Péter sétány 1/A, Budapest H-1117, Hungary; [2]Max Planck Institute for the Physics of Complex Systems, Nöthnitzer Str. 38, Dresden 01187, Germany; [3]Biological Research Centre, Temesvári krt. 62, Szeged H-6726, Hungary; [4]Department of Botany, Hungarian Natural History Museum, Könyves Kálmán krt. 40, Budapest H-1089, Hungary; [5]Institute for Soil Science and Agricultural Chemistry, Centre for Agricultural Research, Herman Ottó u. 15, Budapest H-1022, Hungary

Author for correspondence:
Imre M. Jánosi
Tel: +36 30 371 6351
Email: imre.janosi@ttk.elte.hu

Received: *27 January 2020*
Accepted: *22 May 2020*

New Phytologist (2020) **228:** 1535–1547
doi: 10.1111/nph.16740

Key words: climate change, daily snow depth anomaly, environmental explanatory variables, flowering time fluctuations, machine learning fit, phenology of bulbous taxa, soil temperature.

Summary

- In order to identify the most relevant environmental parameters that regulate flowering time of bulbous perennials, first flowering dates of 329 taxa over 33 yr are correlated with monthly and daily mean values of 16 environmental parameters (such as insolation, precipitation, temperature, soil water content, etc.) spanning at least 1 yr back from flowering.
- A machine learning algorithm is deployed to identify the best explanatory parameters because the problem is strongly prone to overfitting for traditional methods: if the number of parameters is the same or greater than the number of observations, then a linear model can perfectly fit the dependent variable (observations).
- Surprisingly, the best proxy of flowering date fluctuations is the daily snow depth anomaly, which cannot be a signal itself, however it should be related to some integrated temperature signal. Moreover, daily snow depth anomaly as proxy performs much better than mean soil temperature preceding the flowering, the best monthly explanatory parameter.
- Our findings support the existence of complicated temperature sensing mechanisms operating on different timescales, which is a prerequisite to precisely observe the length and severity of the winter season and translate for example, 'lack of snow' information to meaningful internal signals related to phenophases.

Introduction

To optimize flowering time, taxa have evolved various signalling systems to integrate environmental information such as photoperiod and temperature into their developmental programmes. In order to prevent premature flowering, several taxa that adapted to temperate climate need a long cold period for flowering (vernalization). As vernalization evolved many times independently, the molecular mechanisms of winter memory can be quite different for various taxa (Bouché *et al.*, 2017).

Long-time precise phenological documentations are scarce, except for some historical datasets like cherry tree flowering in Japan (Aono & Kazui, 2008). Nowadays, by exploiting developed meteorological observations, continuous efforts have been made to explore relationships between weather parameters and phenophases to optimize for example, sowing times of economically important taxa (e.g. Harding *et al.*, 1976; Zheng *et al.*, 2012; Aguilera *et al.*, 2015; Hur & Ahn, 2017; Flynn & Wolkovich, 2018). Large species pools of wild-growing taxa, often kept in ornamental gardens, were also subjected to long-term phenological studies. Several reports have shown that global climate change can significantly alter numerous phenophases including flowering. The general conclusion of these studies is that in mid-latitude geographic locations the global climate change leads to the shortening of flowering duration and to the advance of first flowering dates (Tooke & Battey, 2010), the transformation of vegetation (including disappearance of native species and appearance of invaders), the disruption of synchronous biological interactions and a decline in biodiversity (e.g. White, 1979; Fitter *et al.*, 1995; Fitter & Fitter, 2002; Miller-Rushing *et al.*, 2008; Amano *et al.*, 2010; Bock *et al.*, 2014). Most explanatory studies concluded that monthly average temperatures of preceding seasons exhibit the best correlation with flowering data (White, 1979; Fitter *et al.*, 1995; Amano *et al.*, 2010). Nevertheless, snowpack, frost events, growing degree days, soil temperature and mean sunshine strength and duration (White, 1979; Inouye & McGuire, 1991; Tooke & Battey, 2010; Carbognani *et al.*, 2016; Wadgymar *et al.*, 2018), or complex meteorological patterns like La Niña episodes (Inouye *et al.*, 2002) and North Atlantic Oscillations (Templ *et al.*, 2017) were also considered in some studies. In order to make statistical analyses feasible by traditional methods, all of these studies evaluated a restricted number of aggregated environmental variables (typically, monthly or seasonal mean values) to explain phenological

This article is dedicated to the memory of Dr Szaniszló Priszter (1917–-2011), the former director of the Botanical Garden, Eötvös Loránd University, Budapest, Hungary.

changes. This approach is also based on the logical assumption that taxa grow in strongly fluctuating environments, therefore to minimize inadequate responses, they use long-term weather information to adjust flowering time.

In this work we evaluate historical records of first flowering days of 329 bulbous perennial taxa (298 species or subspecies and 31 further taxa belonging to 49 genera, mostly *Tulipa*, *Allium*, *Muscari*, *Crocus* and *Ornithogalum*) in the period 1968–2001. (Here the term 'bulbous' is used in a broad sense referring to nonrelative taxa that survive winter by means of various underground organs commonly mentioned as 'bulbs'.) We correlate first flowering day fluctuations with meteorological records at monthly and daily temporal resolutions. The new aspect in our approach is that instead of reducing the number of potential explanatory parameters by, for example, computing monthly mean values and restricting their number by some anticipated hypotheses, we exploit all the information of 16 environmental variables with daily temporal resolution covering several months prior to the flowering date. These parameters are not independent, strong correlations are naturally arising because of obvious couplings between cloud cover and precipitation, net solar radiation and temperature, etc. The fitting of a short flowering time series (maximum 33 data points) by several hundreds of input variables is obviously an overdetermined mathematical problem for any traditional method. However, the developing concept of machine learning (e.g. Li *et al.*, 2015; Czernecki *et al.*, 2018) provides an appropriate tool to tackle such a redundant task by unambiguously identifying the most relevant explanatory variables.

Materials and Methods

Plant data and study site

Flowering data were collected between 1968 and 2001 by Dr Szaniszló Priszter (1917–2011, the former director of the Botanical Garden, Eötvös Loránd University, Budapest, Hungary). He recorded 'first flowering days', which is the day when the first plant individual of a given taxon blooms in a given year. The geographic location of the study site is Pék utca 7., Budapest, Hungary, 47.4413°N, 19.0179°E, elevation 122 m, the home garden of Dr Priszter. Here he planted 329 taxa (298 species or subspecies and 31 further taxa) of his favourite (mostly bulbous) perennials. The species belonged to 49 genera of which *Tulipa*, *Allium*, *Muscari*, *Crocus* and *Ornithogalum* were the most represented. The vast majority of taxa (except those having cultivar epithet) were collected from their original habitats during botanical expeditions by Dr Priszter and his colleagues in the Balkans, Turkey, Caucasus Mountains and Tian Shan Mountains. Other taxa were ordered from botanical gardens located within the natural distribution range of the given taxon via germinule exchange programmes. The list of taxa sorted by an increasing mean flowering day of year is given in Supporting Information Table S1. Missing data occur for several reasons: the species failed to flower that year, the flower buds were damaged causing uncertainty in identifying the first day of flowering, it is planted later than 1968 (for the taxa that have missing data in the early years but continuous record later), or Dr Priszter might not have been present in a few cases.

Robust linear fits of trends

We applied the robust linear fit procedure 'scipy.stats.mstats.theilslopes' based on the Theil–Sen estimator (Sen, 1968) and implemented in the SciPy library in Python environment (Millman & Aivazis, 2011). The regression algorithm computes the slope as the median of all slopes between all possible $(x_i,y_i) - (x_j,y_j)$ paired values (for 33 points in a time series, the total number of independent pairs is the combination $33!/[2!(33-2)!] = 528$, where '!' denotes factorial). It also returns the bounds of the confidence interval of a prescribed (input) value, usually 95%. The estimator can be computed efficiently, and it is insensitive to outliers.

Environmental parameters

Time series of high temporal resolution (6 h) were evaluated for the period 1 January 1958–31 December 2000 from the ERA-40 reanalysis data bank compiled and maintained by the European Centre for Medium-Range Weather Forecast (Uppala *et al.*, 2005). (Note that this interval of 44 yr is 11 yr longer than flowering data, however we used the whole set for obtaining statistical properties.) As a first step, daily mean values were determined, altogether 16 071 data points for 16 environmental variables (see Table 1; Supporting Information Fig. S1). The geographic grid cell of spatial extent 0.125° × 0.125° at the position 47.5°N (latitude), 19.0°E (longitude) is only 6.7 km away from the location of the garden where flowering data are recorded (see earlier). Nevertheless, we performed consistency tests over an extended area around the target point (see Fig. S2). Fig. S3 Illustrates the climatological mean determined for each calendar day and for each variable, leap days are not omitted. Fig. S4 demonstrates the spatial homogeneity of the meteorological fields: daily fluctuations of the difference between the central grid point and the spatial mean are almost negligible. The environmental variables are obviously not independent, real-time cross-correlations are visualized in Fig. S5. Time dependent cross-correlations (Fig. S6) reveal well known temporal lags between variables, for example that mean temperature lags behind net solar radiation by 20 d (at this geographic location).

We tested 16 variables from the ERA-40 reanalysis data bank at daily temporal resolution (see Table 1; Fig. S1). Monthly mean values are also determined and evaluated. The data set contains a precipitation group (three variables), insolation group (three variables), temperature group (two levels in air + two levels in soil), snow depth, total cloud cover, and volumetric soil water (four levels), see Table 1. Ambient temperature (growing degree days), solar radiation (day length), and drought stress related to the lack of precipitation and depleted soil water are known to fundamentally affect flowering time (Cho *et al.*, 2017; Singer, 2018; Wadgymar *et al.*, 2018), snow depth and total cloud cover are incorporated for the sake of comprehensiveness.

Table 1 Variables tested from the ECMWF ERA-40 reanalysis data bank.

No.	Notation	Long name	Units
1	*p1*	Convective precipitation	cm
2	*p2*	Stratiform (large-scale) precipitation	cm
3	*p3*	Total precipitation (*p1* + *p2*)	cm
4	s1	Surface net solar radiation	W m^{-2}
5	*s2*	Surface solar radiation downwards	W m^{-2}
6	*s3*	Daily sunshine duration	h
7	*t1*	2 m temperature	°C
8	*t2*	Skin temperature	°C
9	*t3*	Soil temperature, level 1: 0–7 cm downwards	°C
10	*t4*	Soil temperature, level 2: 7–28 cm downwards	°C
11	sn	Snow depth	cm (of water equi.)
12	tcc	Total cloud cover	Fraction [0–1]
13	sw1	Volumetric soil water, layer 1: 0–7 cm downwards	m^3 m^{-3}
14	sw2	Volumetric soil water, layer 2: 7–28 cm downwards	m^3 m^{-3}
15	sw3	Volumetric soil water, layer 3: 28–100 cm downwards	m^3 m^{-3}
16	sw4	Volumetric soil water: layer 4: 100–289 cm downwards	m^3 m^{-3}

The native temporal resolution is 6 h, we computed daily and monthly mean values, climatological means, and anomalies for the whole period of 1 January 1958–31 December 2000.

Using the 44 yr long meteorological records, mean values of all 16 climatological variables were determined for each calendar day (see Fig. S3) and for each calendar month (daily and monthly climatological mean values). Besides the direct records, anomaly time series were also used as potential explanatory variables. Daily anomaly is defined as the difference between the recorded value of a variable on a given day and the climatological mean value on the same calendar day (Fig. S7). Monthly anomalies were calculated by the same procedure: a given monthly climatological mean value of a variable is subtracted from the actual monthly mean of the record (Fig. S8). Note that the removal of climatological means does not affect existing long-term tendencies: when an average calculated over systematically decreasing values in consecutive years is subtracted, the trend obviously remains.

Tests of spatial homogeneity resulted in that the closest grid point (6.7 km away from the garden where flowering data are recorded) is representative enough (see Fig. S4, and compare the horizontal scales representing spatial variability with the vertical scales of the signals in Figs S1 or S3), therefore spatial extrapolation was not necessary.

Orthogonal matching pursuit (OMP) fitting procedure

In general, a machine learning problem considers a set of samples and attempts to predict properties of unknown data. Our implementation falls into the category of 'supervised learning', where the main task is to find a function that maps an input to an output based on example pairs of an input object (in our case, vectors of meteorological variables) and an output value (first flowering day, the supervisory signal). The usual approach of testing a given algorithm is data splitting, where the training set is used to estimate the mapping function, and the test set is used to evaluate predictive capacity. Since we have here a supervisory signal of pretty restricted length (maximum 33 data points for a specific taxon), we do not explore real prediction, we exploit the first part of the procedure, learning. Namely, we use supervised learning to find an optimal estimator explaining year-by-year fluctuations of flowering days individually for all taxa represented in our data base. Usually, machine learning outperforms traditional methods, especially for sparse data (lots of missing data points). One of the most often quoted disadvantage of machine learning algorithms is the problem of interpretability ('black box' aspect): it is often not clear, how and why an algorithm produces model parameters providing very nice fits/predictions but lacking a transparent understanding. As we will demonstrate, our linear regression falls into the interpretable model category (Molnar, 2019), and provides nontrivial outcomes by analysing the results.

In order to identify possible relationships between the environmental variables and flowering dates, we performed multivariate linear regression analyses by several methods provided by the Python Scikit-Learn toolbox (https://scikit-learn.org/; Pedregosa *et al.*, 2011) ('scikit-learn v.0.20.2'). Detailed comparisons of regression efficiencies unambiguously guided us to the implementation of the 'orthogonal matching pursuit' (OMP) algorithm (Tropp *et al.*, 2006). OMP is a sparse approximation procedure which aims to find the 'best matching' projections of multidimensional data onto an over-complete (redundant) set of independent variables ('importance fit'). The method has been developed for signal recovery from incomplete and inaccurate measurements (Tropp *et al.*, 2006; Tropp & Gilbert, 2007), however it has been proven to be a very efficient tool also in bioinformatics (Misof *et al.*, 2014; Biswas *et al.*, 2017) or image processing (Choukroun *et al.*, 2018; Zhao *et al.*, 2018). Note that the key input parameter of the algorithm is the required number of nonzero coefficients *FitVar*.

The algorithm provides the best possible linear fit, where the target time series (standardized flowering day $Z_{\mathrm{fd},i}(Y)$ of taxon i in year Y) is expressed as a linear combination of explanatory parameters (external meteorological variable anomaly x_j) as:

$$Z_{\mathrm{fd},i}(Y) = a_0 + a_1x_1 + a_2x_2 + \cdots + a_nx_n,$$

where $\{a_0, a_1, \cdots a_n\}$ are fitted coefficients, and the number of variables $FitVar = n$ is a prescribed value. For example, in the case of $FitVar = 2$, the result is one or two environmental parameters on two particular days or months (in case of monthly mean values) providing the best linear fit. The stability of a given fit can be checked by changing the length of historical weather data L prior to the flowering in a particular year, and the number of input data sets N (the number of years evaluated). According to our results, the required length $L_{\min}$ should contain at least *c.* 100 d from the preceding year, thus a weather history of *c.* 400 d is necessary in case of the late flowering species. As for N, the fit for snow depth anomaly remains stable (the same days are chosen) when the number of years is larger than about 25.

The OMP algorithm does not require even sampling at all, when it is used to fit time series. Therefore, missing data is handled simply by omitting those years when flowering records are not available (white squares in Fig. 1).

Statistical evaluation

Regression qualities are evaluated by the usual coefficient of determination R^2, which is the proportion of the variance in the dependent variable $\{y_i\}$ that is predictable from the independent variables $\{x_i\}$ by the model values $\{f_i\}$:

$$R^2 \equiv 1 - \frac{\sum_i (y_i - f_i)^2}{\sum_i (y_i - \langle y \rangle_i)^2}.$$

Statistical confidence tests

In order to check whether the observed statistical association is a procedural artefact or not, we implemented a data shuffling test. Tests were performed by (1) aligning anomaly records of $L = 360$ d backward from the dates of flowering (day 0 belong to the flowering events), and (2) randomly mixing the indices of years by the PYTHON procedure 'numpy.random.permutation' (NUMPY v.1.9 module). Note that individual time series slices remain intact, days in a given calendar sequence are not shuffled. Such randomly reordered whole year meteorological records served as input data for OMP fitting. The result is shown in Fig. S9. The consistent distribution of symbols below the diagonal indicates that indeed the weather signal in the particular year is reflected in flowering day fluctuations, thus the variability of flowering dates is not simply the result of deterministic seasonality with some random noise.

Data availability

The flowering data set is available upon request from P. C. (email: cspeter@rissac.hu).

Results

Decadal trends of flowering time

Fig. 1 illustrates the flowering data set sorted by an increasing order of the mean flowering day of year (for the full list of taxa see Table S1). Apparent horizontal colour stripes indicate strong coherent anomalies when a group of taxa exhibits either a delayed or an early onset of flowering with respect to the mean date over the given period of 33 yr. For an appropriate comparison, the flowering time series of each taxon is standardized as usual:

$$Z_{\mathrm{fd},i} = \frac{\mathrm{Fd}_i(y) - \langle \mathrm{Fd}_i \rangle_y}{\sigma_{\mathrm{fd},i}}, \qquad \text{Eqn 1}$$

where $\mathrm{Fd}_i(y)$ is the flowering day of year for taxon i in a given year y, angle brackets denote mean value over the whole record, and $\sigma_{\mathrm{fd},i}$ is the standard deviation in units of day.

As taxa of close first flowering days apparently respond in a coherent way to environmental stimuli (Fig. 1), we classified the taxa according to their mean flowering time into monthly groups. The standardized first flowering day of each member of a given group, the ensemble mean flowering time and the calculated robust linear fits are determined for each group (Fig. S10). As an example, we present the May group in Fig. 2. Fig. 2 shows that (1) the first flowering day of the 78 taxa fluctuates rather coherently, (2) the fluctuations are intense, frequently larger than two standard deviations and (3) the overall tendency (blue line in Fig.

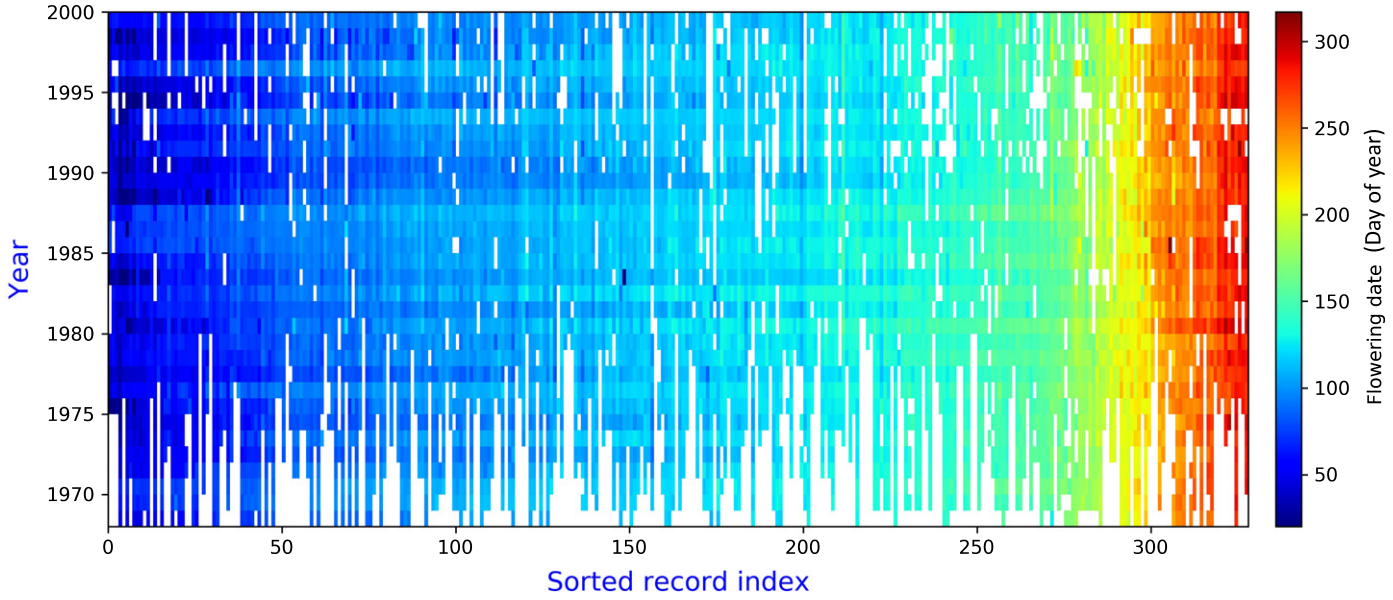

Fig. 1 Graphical representation of the flowering data set. The horizontal axis shows the index of taxa, in an increasing order of the mean flowering day of year, the vertical axis is the year between 1968 and 2000. For the full list of taxa, see Supporting Information Table S1. The flowering date (day of year) is colour coded, white indicates missing data.

2) is a shift to earlier first flowering onset by 2.32 d/decade (it is significant over 95%). Highly significant tendencies of earlier first flowering were also observed for the June group of taxa and less convincingly for the February, March and April groups (Figs S10, S11). By contrast, the August group exhibits significant delaying tendency of flowering onset (Figs S10g, S11). As for trends fitted to individual records (see Table S1), 182 trends are significant at the 68% confidence level (149 negative slopes), while 61 are significant at 95% (50 negative slopes). Similar early flowering tendencies for spring taxa growing under temperate climate as a consequence of global warming are reported several times (Menzel & Fabian, 1999; Sparks & Menzel, 2002; Walther *et al.*, 2002; Parmesan, 2006; Schwartz, *et al.*, 2006; Tooke & Battey, 2010; Jones & Daehler, 2018; Renner & Zohner, 2018; Park *et al.*, 2018; Singer, 2018). It was also shown that climate change can lead to a delayed autumn flowering in the same geographic region (Menzel & Fabian, 1999; Sparks & Menzel, 2002). Notable, although earlier spring flowering is also an obvious and robust trend in our dataset, none of the individual environmental parameters exhibits a significant tendency at the experimental location (see Fig. S1).

Relevantly, at most groups, the flowering times show intense and coherent fluctuations (Figs 2, S10). These coherent fluctuations are likely triggered off by common fluctuating environmental parameters. In order to identify the most important flowering time modulating external parameters, we analysed the correlations between various meteorological records at monthly and daily resolutions and flowering times for each taxon.

Fits of flowering time with monthly mean anomaly time series

The usual approaches of similar phenological studies are based on input data aggregation, in order to restrict the size of potential explanatory parameter set to be tractable. Therefore, at first we performed multivariate linear OMP regression (see the Materials and Methods section) with monthly mean anomaly time series, where climatological mean values are determined separately for each calendar month and subtracted from the original records of monthly means (see Fig. S8). We considered 12 months of weather history for each taxon back from the mean flowering date (the month of mean flowering day is included). In this way, the number of possible explanatory variables is $16 \times 12 = 192$ (number of meteorological variables times the number of months backward from mean flowering), which is overly redundant to fit a time series of maximum 33 first flowering day anomalies.

When the number of permitted nonzero OMP coefficients is as high as $FitVar = 9$, the result is 'noise fitted by noise' with a high quality matching ($\langle R^2 \rangle = 0.945$, see Fig. 3a). The distribution of coefficients among the external variables is almost random, with some preference of convective precipitation ($p1$), $soil_2$ temperature ($t4$), snow depth (sn), and total cloud cover (tcc) (Fig. 3a). The real benefit of the OMP algorithm arises when the number of variables is systematically decreased. Fig. 3(c) illustrates that as few as two explanatory variables work quite well ($\langle R^2 \rangle = 0.613$), furthermore the fits unambiguously converge to monthly mean soil temperature anomalies at the layer depth of 7 to 28 cm ($soil_2$ temperature anomaly, $t4$). Even a single input variable (Fig. 3d) works satisfactorily in many cases, nevertheless the ensemble mean value for the coefficient of determination is not very impressive ($\langle R^2 \rangle = 0.437$), see also Fig. S11. Note that in Fig. 3(d) ($FitVar = 1$), 28 + 17 + 39 + 136 = 220 fluctuating flowering time series (out of 329) can be best fitted by monthly mean temperature anomalies: in the air at 2 m ($t1$), at 0 m ($t2$), in the soil at depths of 0 to 7 cm ($t3$), and 7 to 28 cm ($t4$), respectively.

Fit with $FitVar = 1$ means that a time series of a single external parameter (from the 16) at a given month (from the 12 prior flowering) is chosen by the OMP procedure as the best explanatory variable. The temporal distribution of the two most optimal input parameters (monthly mean $soil_2$ and $soil_1$ temperature anomalies) is illustrated in Fig. 4. Apart from some statistical fluctuations, the emerging picture is that integrated soil temperature information back to at least 1 or 2 months before flowering is essential for bulbous taxa, albeit with a moderate explanatory capacity (see all individual R^2 values in Fig. S12). The negative

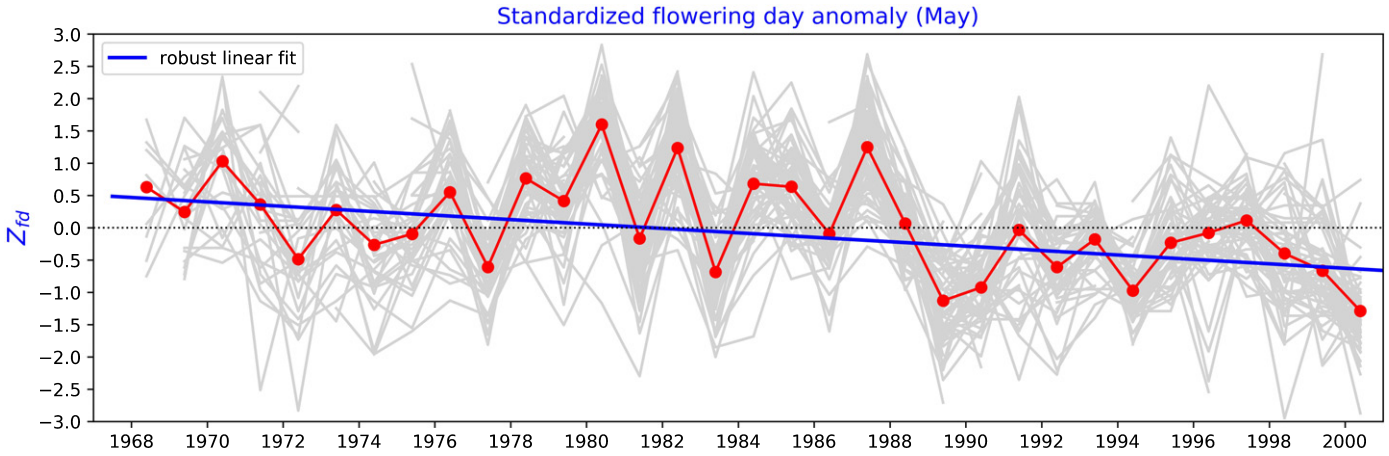

Fig. 2 First flowering day anomalies Z_{fd} for the May group of 78 taxa. Grey lines indicate the individual time series standardized by Eqn 1, red symbols denote the ensemble mean values. The blue line is a robust linear fit (see the Materials and Methods section) of slope −0.029 yr^{-1} with the 95% confidence interval (−0.054, −0.006). Since $\sigma_{fd} = 8.02$ d (May group mean value), the slope of tendency translates to −2.32 d^{-1} decade.

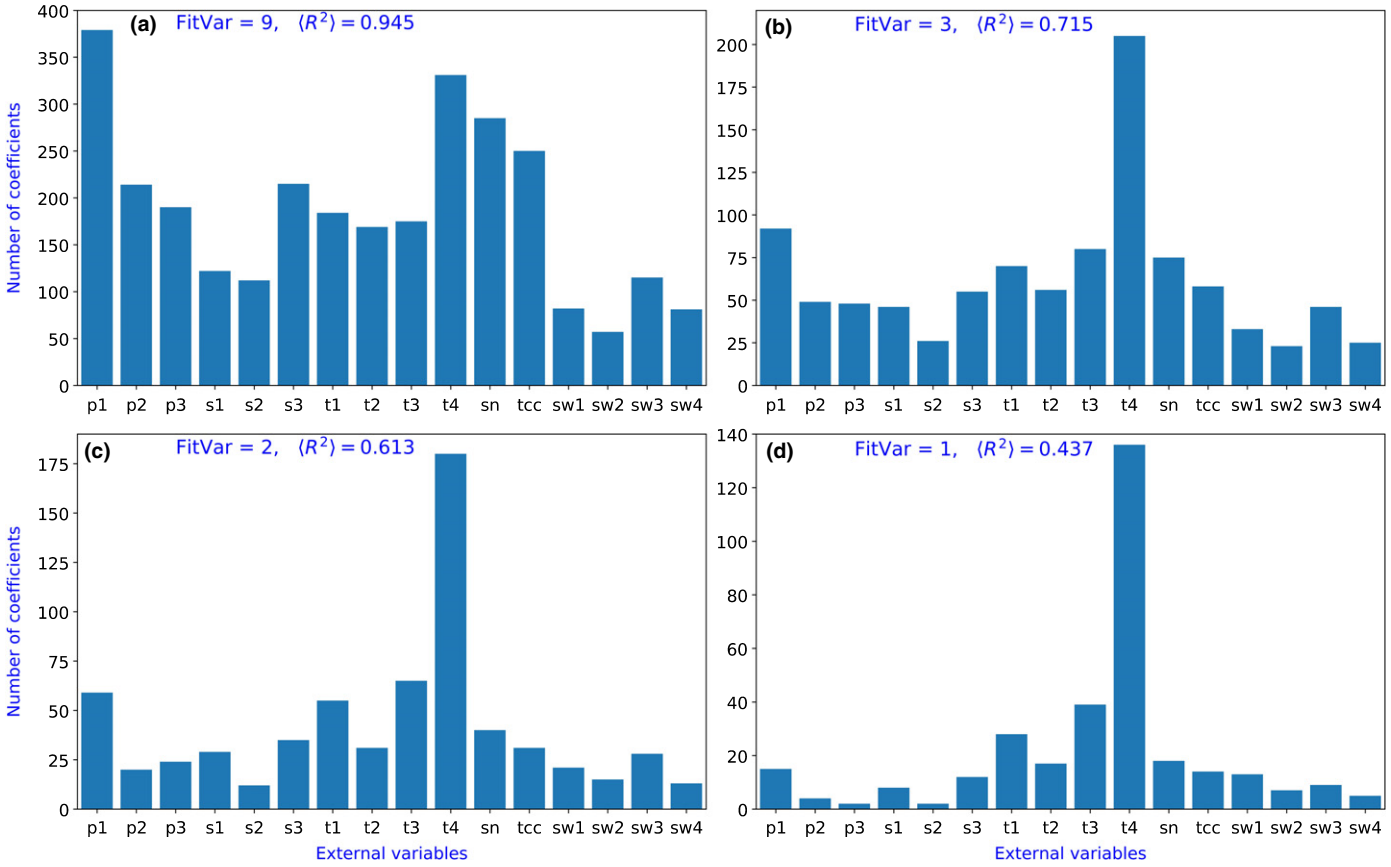

Fig. 3 Summary statistics for nonzero 'orthogonal matching pursuit' (OMP) coefficients at decreasing numbers of permitted fitting parameter *FitVar*. Bar charts illustrate results for 12 months of mean anomaly time series back from flowering date, the labels of the 16 external variables (horizontal axes) are listed in Table 1. The number of prescribed explanatory variables (*FitVar*) is indicated in the legends, together with the ensemble mean value of the coefficient of determination $\langle R^2 \rangle$. The OMP algorithm selects the *FitVar* = *n* best fitting variables to the flowering time anomaly record of each taxon. The vertical axes show how many times a given external variable was selected among the best explanatory variables. (In each panel, the total number of hits is simply 329 × *FitVar*.) (a) *FitVar* = 9, $\langle R^2 \rangle$ = 0.945, (b) *FitVar* = 3, $\langle R^2 \rangle$ = 0.715, (c) *FitVar* = 2, $\langle R^2 \rangle$ = 0.613, and (d) *FitVar* = 1, $\langle R^2 \rangle$ = 0.437.

sign (blue colour) means that an unusually cold spring (negative mean soil temperature anomaly) delays, a warm spring (positive mean soil temperature anomaly) promotes early flowering proportionally with the magnitude of anomalies. These results are in line with previous reports that higher than average temperature during the growth phase results in earlier flowering of bulbous taxa (Khodorova & Boitel-Conti, 2013; Leeggangers *et al.*, 2017). Our data also suggest that soil temperature (especially at bulb depths) is more representative than air temperature, which is consistent with the fact that bulb resources are utilized during the early growth phase. Air and soil temperatures are strongly correlated (see Fig. S5), nevertheless it seems that the dampened fluctuations in the soil are more consistent with the fluctuations of flowering dates.

Fits of flowering time with daily time series

In addition to the correlations between flowering time and monthly mean environmental parameters, we also analysed the relationship between flowering time and daily meteorological records. Using daily data increases the size of input parameter set enormously: one year weather history ($L = 365$) means $16 \times 365 = 5840$ (number of meteorological variables times the number of days backward from flowering date) input time series of length of 33 yr. Since we intended to extract characteristic weather signals with respect to the day of flowering, we shifted the historical weather record segments of length L relative to each other so that the last day corresponded to the first day of flowering in each year (input time series alignment).

Figure 5 illustrates summary statistics of nonzero OMP coefficients for an extended search based on both the original weather records (Fig. 5 left column), and anomaly time series (Fig. 5 right column). Anomalies perform somewhat better as explanatory variables (see the R^2 values). When the number of nonzero coefficients is high enough as *FitVar* = 9, the result is 'noise fitted by noise' again with an almost perfect matching ($\langle R^2 \rangle$ = 0.998, see Fig. 5b). The distribution of coefficients does not exhibit any well-defined pattern, although some preference of total cloud cover (tcc) for the direct records, while convective precipitation ($p1$) and snow depth (sn) for the anomaly series is visible (Fig. 5a,b). Importantly, the systematic decrease of permitted numbers of OMP coefficients unambiguously converges to snow

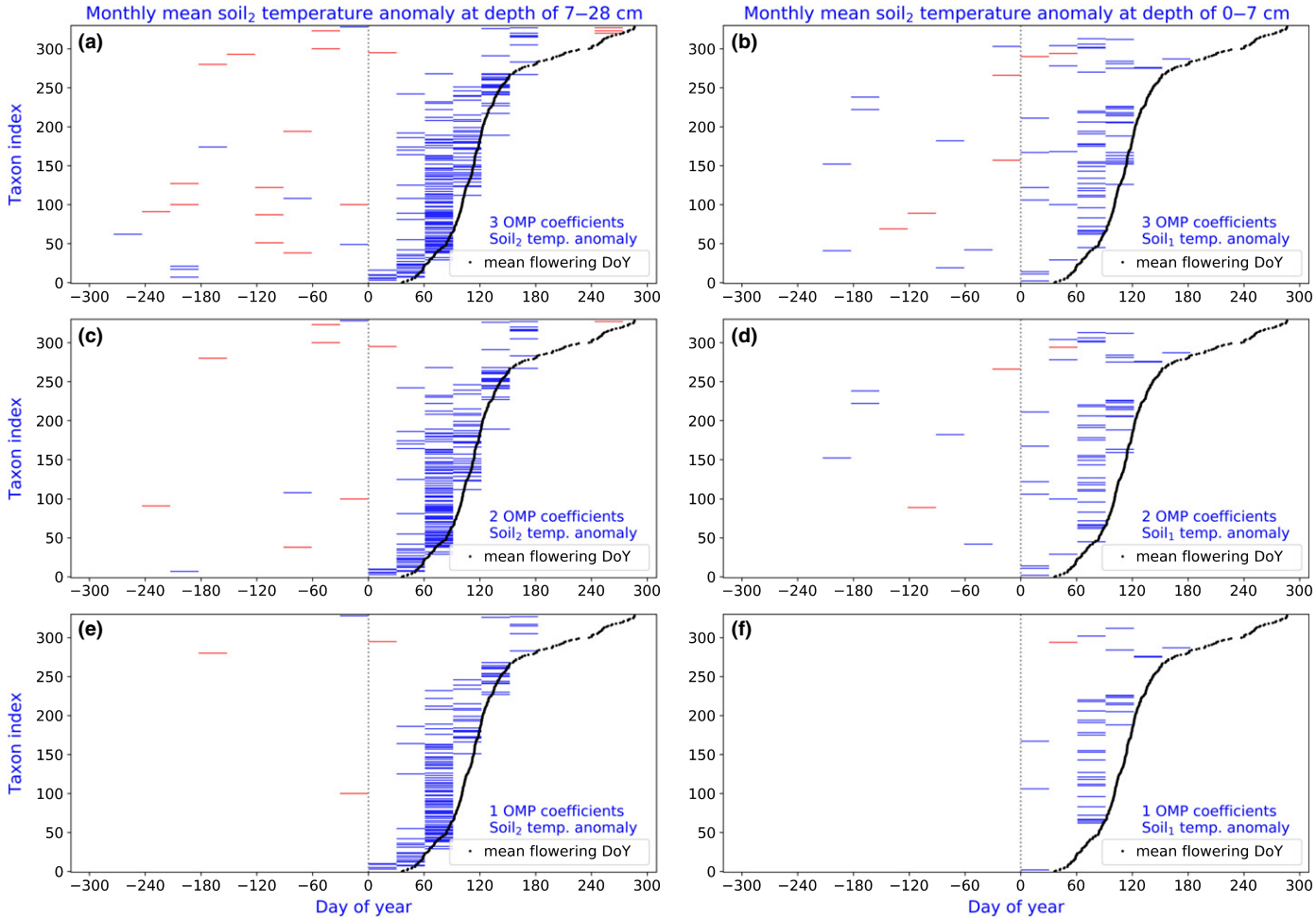

Fig. 4 Ensemble statistics for the temporal distribution of two 'orthogonal matching pursuit' (OMP) parameters. Horizontal axes are measured in units of day (the value zero separates 31 December of the previous, and 1 January of a flowering year); vertical axes denote the taxon index from 1 to 329. Black symbols indicate the mean first flowering day of year for each taxon. Horizontal bars visualize the month of determining mean values. Blue/red colour indicates negative/positive sign of the fitting coefficient. Left column, $soil_2$ (*t4*)-; right column, $soil_1$ (*t3*) temperature, monthly mean anomalies. (a) *FitVar* = 3, parameter *t4*, (b) *FitVar* = 3, parameter *t3*, (c) *FitVar* = 2, parameter *t4*, (d) *FitVar* = 2, parameter *t3*, (e) *FitVar* = 1, parameter *t4*, and (f) *FitVar* = 1, parameter *t3*.

depth anomaly. This result is rather surprising, because the snow depth time series is pretty empty, it is zero on 200–250 d in a year (see Fig. S1k). The dominance of snow depth anomaly is almost full when *FitVar* = 1 is fixed for OMP calculations (see Fig. 5h), 280 flowering time series out of the 329 is explained by means of snow depth anomaly on a particular day before flowering. In case of *FitVar* = 2, 124 flowering records are best fitted by snow depths anomaly on 2 d, and further 168 cases are best fitted by snow depths anomaly and another variable (mostly convective precipitation anomaly, see Fig. 5f). The numbers for *FitVar* = 3 (Fig. 5d) are 43 cases with 3, further 125 cases with 2, and 224 cases with at least 1 snow depth anomaly.

One might expect that the monthly parameters correlate better with flowering fluctuations because adjustment of flowering time requires integration of long-term data. Surprisingly we found the opposite: the explained variance $\langle R^2 \rangle$ is drastically larger for the fits with daily records at the same number of permitted OMP coefficients than that of for fits with monthly mean series (for instance, at *FitVar* = 1, $\langle R^2 \rangle$ = 0.437 and 0.706 for the best monthly and daily parameters, see Fig. S12). This observation might suggest that short time environmental changes affect the flowering programme more significantly than integrated signals. A more likely alternative explanation may be that the snow depth anomaly at a given day is a good proxy for a combination of different parameters such as skin and soil temperatures, soil water content, etc., in the neighbouring days around the time of observation.

In order to demonstrate the exceptional fitting capacity of daily snow depth anomalies, we repeated all the calculations by excluding this variable from the input parameter set. The results in Fig. S13 indicate that the values of the ensemble average of the coefficient of determination $\langle R^2 \rangle$ decreased systematically for *FitVar* = 1, 2 and 3, and the selectivity of the procedure also dropped (e.g. in Fig. S13h, 13 from the 15 input parameters have at least two hits, however in Fig. 5h only three from the 16, with a particularly strong dominance of snow depth anomaly). Direct meteorological records (Fig. S20 left column) now perform somewhat better than anomalies (Fig. S20 right column). An

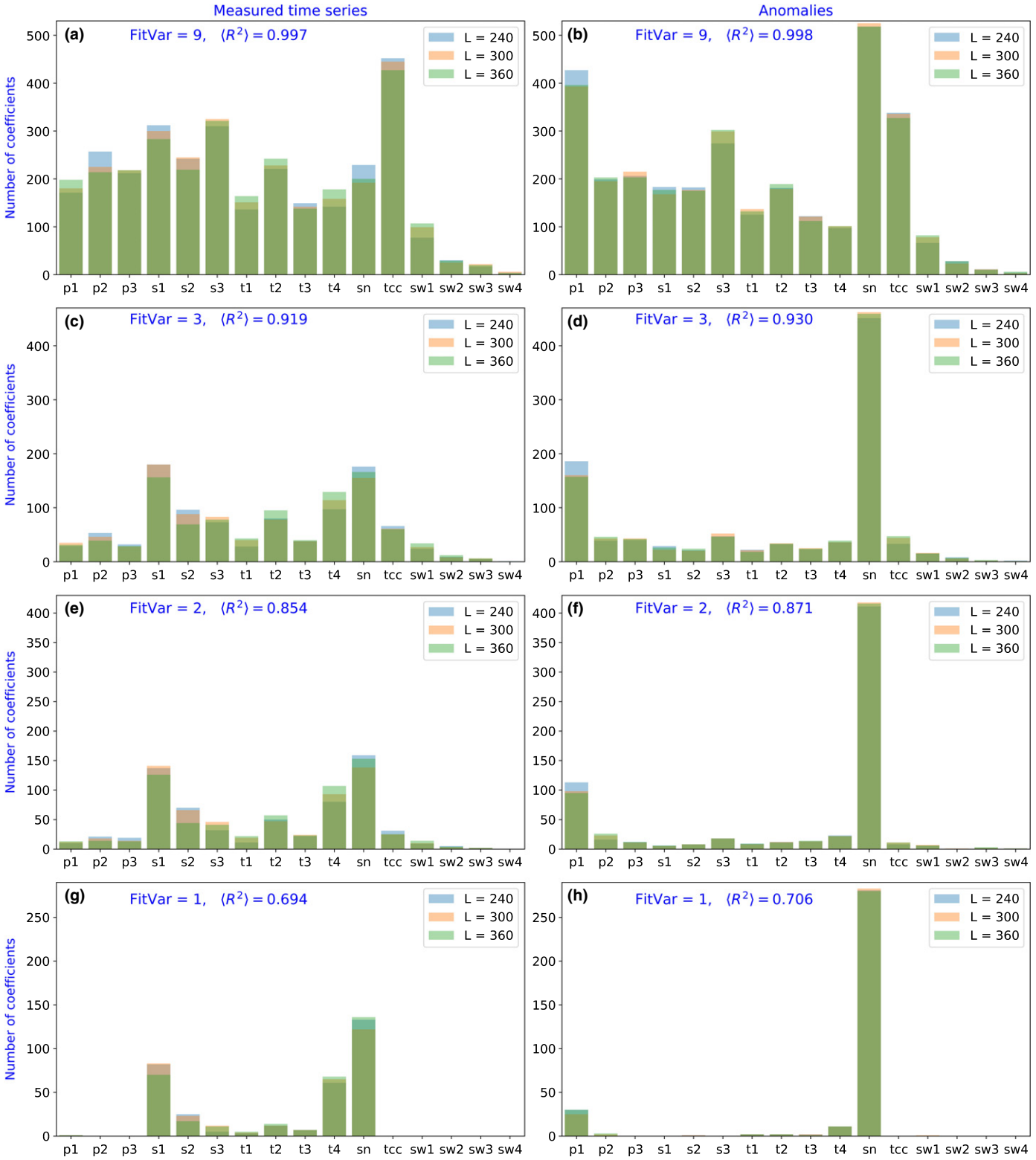

Fig. 5 Summary statistics for nonzero 'orthogonal matching pursuit' (OMP) coefficients at various initial conditions. The left/right columns of four panels illustrate results for direct weather records/anomalies (daily climatological means subtracted). Labels of the 16 external variables (horizontal axes) are listed in Table 1. The predefined number of explanatory variables (*FitVar*) and the ensemble mean value of the coefficient of determination $\langle R^2 \rangle$ are (a) *FitVar* = 9, $\langle R^2 \rangle = 0.997$, (b) *FitVar* = 9, $\langle R^2 \rangle = 0.998$, (c) *FitVar* = 3, $\langle R^2 \rangle = 0.919$, (d) *FitVar* = 3, $\langle R^2 \rangle = 0.930$, (e) *FitVar* = 2, $\langle R^2 \rangle = 0.854$, (f) *FitVar* = 2, $\langle R^2 \rangle = 0.871$, (g) *FitVar* = 1, $\langle R^2 \rangle = 0.694$, and (h) *FitVar* = 1, $\langle R^2 \rangle = 0.706$. Three different history lengths are represented here (L = 240, 300 and 360 d, see legends.) The OMP algorithm selects the *FitVar* = n best fitting variables to the flowering time anomaly record of each taxon. The vertical axes show how many times a given external variable was selected among the best explanatory variables. (In each panel, the integrated number of cases is simply 329 × *FitVar*.)

interesting aspect is the strong preference of the parameter 'convective precipitation' ($p1$) already at $FitVar = 9$ when anomalies are the input variables (without snow depth). Note that convective precipitation anomaly is the second most frequent parameter when all the 16 variables are used in Fig. 5, right column. Notable, a common property shared by convective precipitation and snow depth is the strong seasonality with long breaks between the peaks, see Figs S1, S2, S7. Nevertheless, the difference in the fitting efficiencies are very significant ($\langle R^2 \rangle = 0.706$ with snow depth anomalies, while $\langle R^2 \rangle = 0.561$ without snow depths at $FitVar = 1$).

Example for correlation between flowering time and daily snow depth anomaly

Figure 6 explains the results of OMP fit for a given taxon. Weather history slices of length $L = 240$ d colour coded here backward in time from the first flowering day in each year, and shifted relative to each other resulting in a common time scale (first flowering day is day zero, see Fig. 6a). The weather records of consecutive years represented by the colour stripes are plotted on top of each other, the vertical axis indicates the years. The best fitting two parameters for *Ornithogalum lanceolatum* (mean flowering day of year is 122.7) are the snow depth anomalies at −166 and −35 d backward from the actual flowering date (Fig. 6a,c). Notable, the snow depth anomalies at these days correlate extremely well ($R^2 = 0.923$) with the flowering date anomalies (Fig. 6b,d, for additional examples see Figs S14, S16, S18). These illustrations are not 'cherry-picking' examples, see Fig. S12, where R^2 is plotted for each taxon. As for the signs of the fitting parameters, the negative coefficient at day −166 means that more than average snow at that given day (positive anomaly) correlates with proportionally earlier flowering, while the positive coefficient at day −35 means that flowering is delayed when there is more snow than usual. The simplest explanation would be that more than average snow at days −166 and −35 mean unusually cold temperatures, however, the situation is not so trivial. Fig. 6(e) demonstrates that an appropriate mapping into direct temperature records is far from trivial. The $soil_2$ temperatures of the −166 and −35 d (black symbols in Fig. 6e) are scattered in the calendar over the same range as flowering day fluctuations ($soil_2$ temperature was selected as the best explanatory monthly parameter, see earlier). Neither day has any characteristic threshold temperature or temperature gradient (Fig. 6e). Similarly, we could not figure out any simple aggregation scheme of daily temperature data (Fig. 6f) in order to explain the success of snow depth anomaly as explanatory variable for flowering fluctuations. We speculate that the snow depths anomaly data on these two particular days bear complex weather information at around two critical developmental transition phases, the start of winter phase and the transition to spring growth phase.

Note that direct snow depth records severely underperform compared to snow depth anomaly (see Figs S15, S17), plausibly because anomaly series contain extra 'lack of snow' information as negative values.

Temporal distribution of the fitted OMP coefficients

Figure 7 illustrates the results of ensemble statistics, where the back-transformed dates of the best fitting OMP parameters are plotted for each individual taxon separately. The dominating negative sign distributed mostly during the month of preceding November means that for most taxa early snow (positive anomaly) promotes earlier flowering. The exclusively positive sign in March and April is the opposite: as expected, late snow delays flowering. One notable point here is that the 280 taxa (out of 329) fitted successfully by a single snow depth anomaly record on a particular day backward from flowering (Fig. 7c, $FitVar = 1$) exhibit the same critical 'sampling' period (late autumn or early spring) as in the cases of more OMP explanatory parameters (Fig. 7a,b). Furthermore, it is remarkable that bulbous perennials flowering very early or from June to as late as in September and October apparently adjust the day of flowering according to 'the beginning' and 'the end' of the previous winter season (see Figs 7c, S14, S16 for individual examples). For taxa flowering between March and June the most important parameter is the negative snow depth anomaly during spring (Fig. 7c, $FitVar = 1$, and Fig. S19). However, when two parameters are allowed (Fig. 7b, $FitVar = 2$), the second selected snow depths day is in almost every case is a 'late autumn day' in the previous year and not another spring day. Similarly, the second parameter for taxa between June and October is the spring snow depth anomaly. Taken together, we have found that for most taxa (such as was shown in Figs 6, S14, S16, S18–S20) the two best explanatory variables determining flowering dates are a late autumn and an early spring snow depths anomaly.

Discussion

Our main results can be summarized as follows. (1) The OMP algorithm successfully identified the soil temperature anomaly at rooting depth (7–28 cm) as the best monthly mean value and snow depth anomaly as the best daily parameter to explain flowering date fluctuations. (2) It is remarkable that only 2 d, a late autumn and an early spring day in the aligned snow depth anomaly records fit flowering day fluctuations with a surprising accuracy. (3) Apparently most of the 329 taxa, irrespectively of their mean flowering time, tune the precise flowering date according to the previous winter period.

Since most environmental parameters fluctuate strongly, taxa cannot adjust flowering time according to daily weather. Instead taxa incorporate long-term weather information into their flowering regulation, for example, *Arabidopsis* vernalization is known to depend on the number of cold days (Hepworth *et al.*, 2018). Therefore, it is plausible to look for correlations between flowering time and longer term weather parameters such as monthly mean values. However, we found that daily weather parameters explain much better flowering time fluctuations than any monthly value. Taken into consideration that monthly mean parameters exhibit moderate changes from 1 yr to the other, while flowering time fluctuates with very high amplitudes (Fig. 2), from a statistical point of view it is not surprising that

New Phytologist

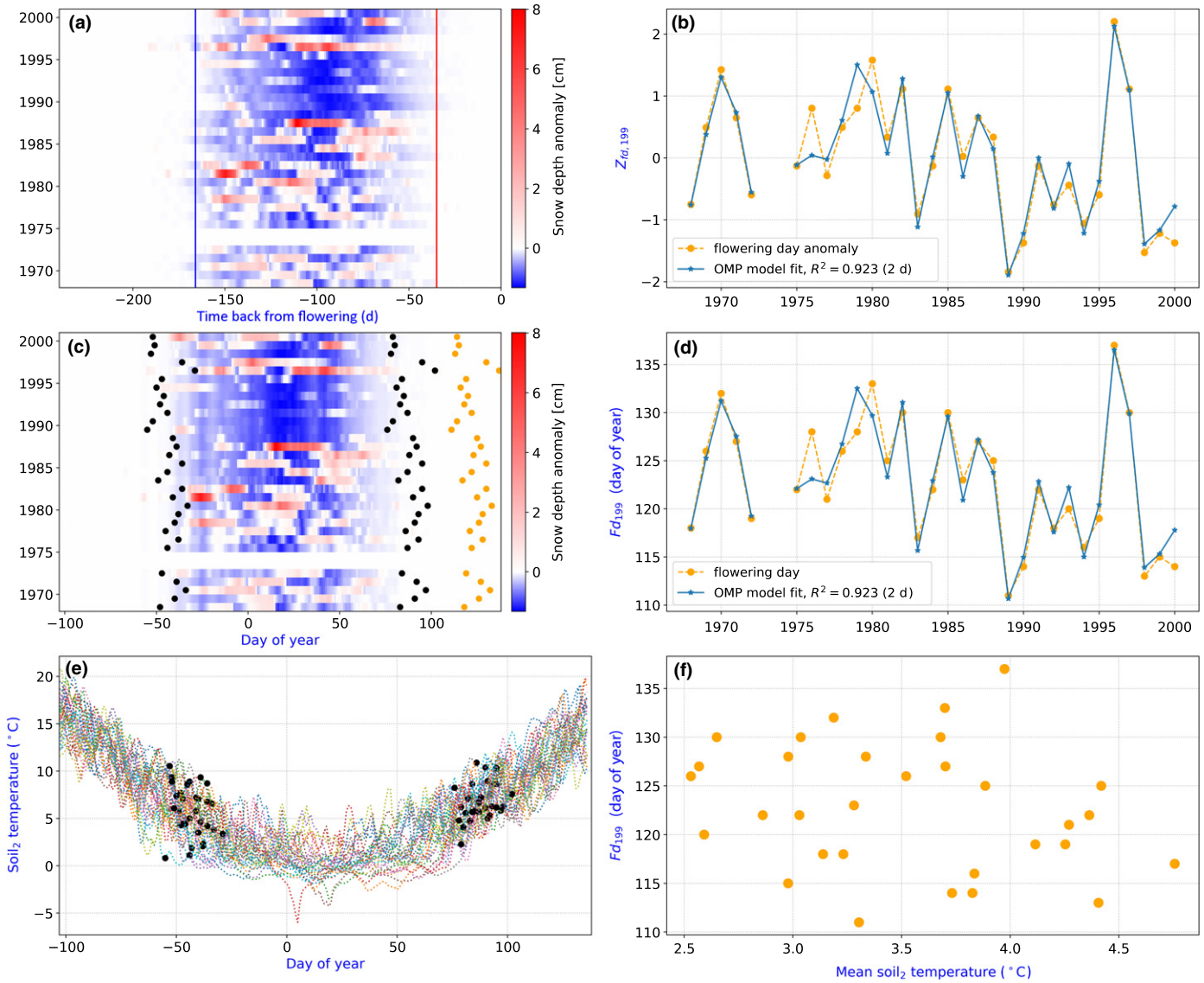

Fig. 6 Illustration of the 'orthogonal matching pursuit' (OMP) regression for taxon index 199 (*Ornithogalum lanceolatum*). (a) Time series of length $L = 240$ d are aligned backward from the day of flowering; snow depth anomalies are colour coded. The weather records of consecutive years represented by the colour stripes are plotted on top of each other, the vertical axis indicates the years. *FitVar* = 2, the 2 d for the best fit are indicated by vertical lines, blue/red for negative/positive coefficient. (b) Illustration of the standardized flowering anomaly series (orange) and the fit by the two variables (blue). The gap indicates missing data (see Fig. 1). (c) Transformation of (a) back to calendar days. The dates corresponding to the vertical lines in (a) are indicated by black symbols, flowering dates are orange. (d) Flowering dates and fitted values in units of day of year. (e) Time series of $soil_2$ temperatures (7–28 cm) during the winter period. Black symbols indicate daily temperatures at the same dates as in (c). (f) An attempt to relate mean $soil_2$ temperatures determined over the 131 d between the fitted dates in (c) and flowering day anomalies.

monthly mean values are weaker explanatory parameters. An unexpected finding is that daily snow depth anomaly is by far the best explanatory parameter.

We can easily exclude that bulbs somehow measure snow depths, not to mention 'lack of snow'. Instead we propose that snow depth anomaly is an integrative parameter that is informative about the soil weather condition of several days at around the observation (an appropriate proxy). As most taxa have evolved in seasonally oscillating environments, their molecular systems of environmental responses are adapted to seasonal changes (Kudoh, 2016; Nagano *et al.*, 2019). Recent results by Hepworth *et al.* (2018) and especially Antoniou-Kourounioti *et al.* (2018) suggest the existence of a complicated temperature sensing machinery (in *Arabidopsis*). Prolonged cold is also important for normal growth and flowering for bulbous taxa (Khodorova & Boitel-Conti, 2013). However, it is likely that the molecular mechanism of vernalization and its role in flowering adjustment is quite different. In *Arabidopsis*, the winter cold is mainly required to down-regulate FLC (*Flowering Locus C*) flowering repressor (Bouché *et al.*, 2017; Antoniou-Kourounioti *et al.*, 2018; Hepworth *et al.*, 2018), while the molecular mechanisms of vernalization are different in bulbous taxa (Lee *et al.*, 2013; Lazare *et al.*, 2019; Wang *et al.*, 2019). However, it was also suggested that increased auxin sensitivity of the bulb induced by a long cold period is a critical

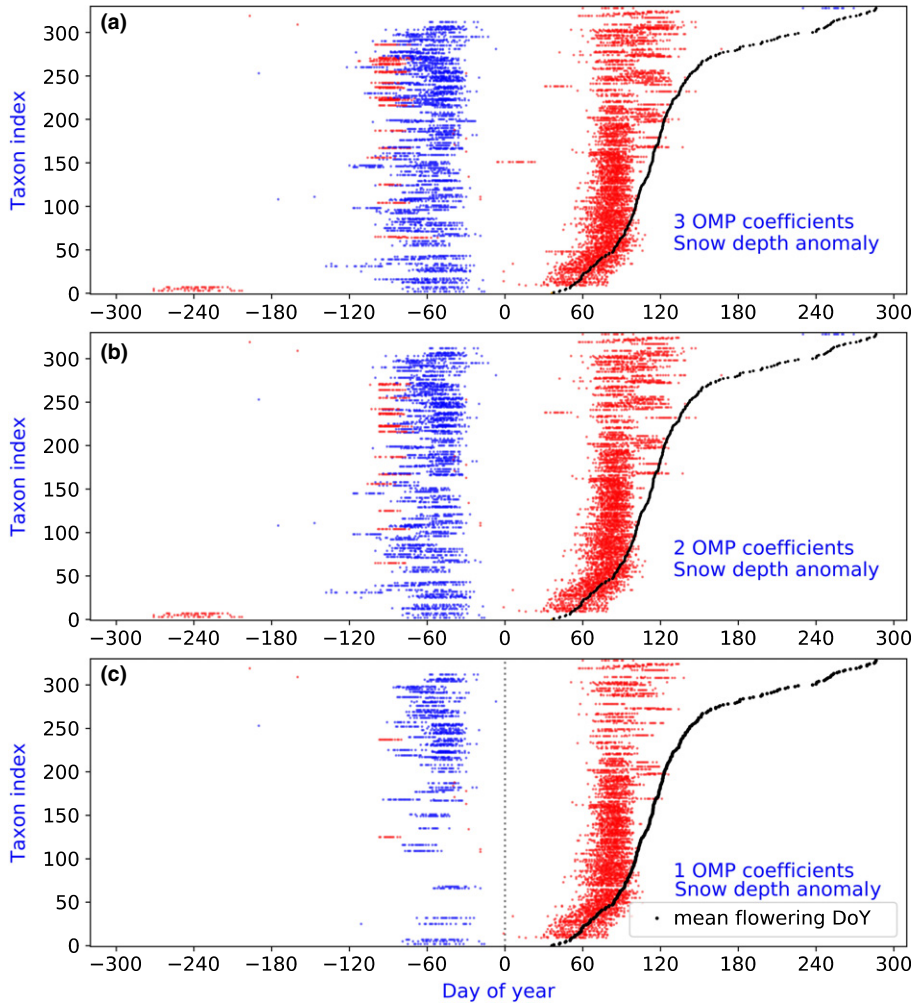

Fig. 7 Ensemble statistics for the calendar day distribution of fitted 'orthogonal matching pursuit' (OMP) parameters for daily snow depth anomaly. Weather history of $L = 360$ d was used for all the individual fits for the 329 taxa (taxon index is on the vertical axes. Blue/red dots indicate negative/positive coefficients; black dots indicate the mean flowering dates. (a) *FitVar* = 3, (b) *FitVar* = 2, and (c) *FitVar* = 1.

common element for the vernalization of several bulbous taxa (Khodorova & Boitel-Conti, 2013). Nevertheless, it seems to be plausible that an elaborated sensory network of long-term memory and effective noise filtering is also necessary for bulbous taxa to precisely detect the extent of the winter season. In the absence of information about key details considering the 329 taxa in our sample, we attempted to find simple combinations of external parameters, computed averages, gradients and running means, tested integration schemes with long-time and short-time kernels, temperature aggregation by fading 'memory', weights depending on the distance back from the flowering date, integration and daily fluctuations added together, etc., in order to best approximate the fitting success of snow depth anomaly records. Up to now, all such attempts are unsuccessful.

In summary, we found that daily snow depth anomalies on as few as 1–3 d sometimes weeks or months before blossoming provide the best explanatory variables to fit year-by-year fluctuations of first flowering days. Obviously, plants (especially bulbous taxa) cannot 'measure' snow depth, or even lack of snow. When daily snow depth anomalies are chosen by the OMP algorithm as best fitting parameters, the particular days coincide with the onset and end of the winter season. This suggests that daily snow depth anomaly is a proxy of a complex temperature signal integrating vital information about the length and severity of the winter period.

Acknowledgements

This work was supported by the Hungarian National Research, Development and Innovation Office (NKFIH) under grants K125171, K129177 and FK125024. and by the Max-Planck Institute for the Physics of Complex Systems in the framework of an Advanced Study Group on 'Forecasting with Lyapunov Vectors'. The authors declare no competing interests.

Author contributions

IMJ designed the research; IMJ and PC performed the research; JT and PC contributed to new methodological/analytical tools; IMJ, DS, JT and PC analysed data; and IMJ, DS and PC wrote the article.

ORCID

Imre M. Jánosi https://orcid.org/0000-0002-3705-5748
Dániel Silhavy https://orcid.org/0000-0002-3370-7067

References

Aguilera F, Fornaciari M, Ruiz-Valenzuela L, Galán C, Msallem M, Dhiab AB, la Guardia CD, Del Mar Trigo M, Bonofiglio T, Orlandi F. 2015. Phenological models to predict the main flowering phases of olive (*Olea europaea* L.) along a latitudinal and longitudinal gradient across the Mediterranean region. *International Journal of Biometeorology* **59**: 629–641.

Amano T, Smithers RJ, Sparks TH, Sutherland WJ. 2010. A 250-year index of first flowering dates and its response to temperature changes. *Proceedings of the Royal Society B* **277**: 2451–2457.

Antoniou-Kourounioti RL, Hepworth J, Heckmann A, Duncan S, Qüesta J, Rosa S, Säll T, Holm S, Dean C, Howard M. 2018. Temperature sensing is distributed throughout the regulatory network that controls FLC epigenetic silencing in vernalization. *Cell Systems* **7**: 643–655.

Aono Y, Kazui K. 2008. Phenological data series of cherry tree flowering in Kyoto, Japan, and its application to reconstruction of springtime temperatures since the 9th century. *International Journal of Climatology* **28**: 905–914.

Biswas S, Kerner K, Teixeira PJPL, Dangl JL, Jojic V, Wigge PA. 2017. Tradict enables accurate prediction of eukaryotic transcriptional states from 100 marker genes. *Nature Communications* **8**: 15309.

Bock A, Sparks TH, Estrella N, Jee N, Casebow A, Schunk C, Leuchner M, Menzel A. 2014. Changes in first flowering dates and flowering duration of 232 plant species on the island of Guernsey. *Global Change Biology* **20**: 3508–3519.

Bouché F, Woods DP, Amasino RM. 2017. Winter memory throughout the taxon kingdom: different paths to flowering. *Plant Physiology* **173**: 27–35.

Carbognani M, Bernareggi G, Perucco F, Tomaselli M, Petraglia A. 2016. Micro-climatic controls and warming effects on flowering time in alpine snowbeds. *Oecologia* **182**: 573–585.

Cho LH, Yoon J, An G. 2017. The control of flowering time by environmental factors. *The Plant Journal* **90**: 708–719.

Choukroun Y, Pai G, Kimmel R. 2018. Sparse approximation of 3D meshes using the spectral geometry of the Hamiltonian operator. *Journal of Mathematical Imaging and Vision* **60**: 941–952.

Czernecki B, Nowosad J, Jabłońska K. 2018. Machine learning modeling of taxon phenology based on coupling satellite and gridded meteorological dataset. *International Journal of Biometeorology* **62**: 1297–1309.

Fitter AH, Fitter RSR. 2002. Rapid changes in flowering time in British plants. *Science* **296**: 1689–1691.

Fitter AH, Fitter RSR, Harris ITB, Williamson MH. 1995. Relationships between first flowering date and temperature in the flora of a locality in central England. *Functional Ecology* **9**: 55–60.

Flynn DFB, Wolkovich EM. 2018. Temperature and photoperiod drive spring phenology across all species in a temperate forest community. *New Phytologist* **219**: 1353–1362.

Harding PH, Cochrane J, Smith LP. 1976. Forecasting flowering stages of apple varieties in Kent, England, by the use of meteorological data. *Agricultural Meteorology* **17**: 49–54.

Hepworth J, Antoniou-Kourounioti RL, Bloomer RH, Selga C, Berggren K, Cox D, Harris BRC, Irwin JA, Holm S, Säll T *et al.* 2018. Absence of warmth permits epigenetic memory of winter in Arabidopsis. *Nature Communication* **9**: 639.

Hur J, Ahn JB. 2017. Assessment and prediction of the first-flowering dates for the major fruit trees in Korea using a multi-RCM ensemble. *International Journal of Climatology* **37**: 1603–1618.

Inouye DW, McGuire AD. 1991. Effects of snowpack on timing and abundance of flowering in *Delphinium nelsonii* (Ranunculaceae) – implications for climate change. *American Journal of Botanics* **78**: 997–1001.

Inouye DW, Morales MA, Dodge GJ. 2002. Variation in timing and abundance of flowering by *Delphinium barbeyi* Huth (Ranunculaceae): the roles of snowpack, frost, and La Nina, in the context of climate change. *Oecologia* **130**: 543–550.

Jones CA, Daehler CC. 2018. Herbarium specimens can reveal impacts of climate change on plant phenology; a review of methods and applications. *PeerJ* **6**: e4576.

Khodorova NV, Boitel-Conti M. 2013. The role of temperature in the growth and flowering of geophytes. *Plants* **2**: 699–711.

Kudoh H. 2016. Molecular phenology in plants: *in natura* systems biology for the comprehensive understanding of seasonal responses under natural environments. *New Phytologist* **210**: 399–412.

Lazare S, Bechar D, Fernie AR, Brotman Y, Zaccai M. 2019. The proof is in the bulb: glycerol influences key stages of lily development. *Taxon Journal* **97**: 321–340.

Lee R, Baldwin S, Kenel F, McCallum J, Macknight R. 2013. FLOWERING LOCUS T genes control onion bulb formation and flowering. *Nature Communications* **4**: 2884.

Leeggangers HACF, Nijveen H, Bigas JN, Hilhorst HWM, Immink RGH. 2017. Molecular regulation of temperature-dependent floral induction in *Tulipa gesneriana*. *Plant Physiology* **173**: 1904–1919.

Li L, Long Y, Zhang L, Dalton-Morgan J, Batley J, Yu L, Meng J, Li M. 2015. Genome wide analysis of flowering time trait in multiple environments via high-throughput genotyping technique in *Brassica napus* L. *PLoS ONE* **10**: e0119425.

Menzel A, Fabian P. 1999. Growing season extended in Europe. *Nature* **397**: 659.

Miller-Rushing AJ, Inouye DW, Primack RB. 2008. How well do first flowering dates measure taxon responses to climate change? The effects of population size and sampling frequency. *Journal of Ecology* **96**: 1289–1296.

Millman KJ, Aivazis M. 2011. Python for scientists and engineers. *Computing in Science & Engineering* **13**: 9–12.

Misof B, Liu S, Meusemann K, Peters RS, Donath A, Mayer C, Frandsen PB, Ware J, Flouri T, Beutel RG *et al.* 2014. Phylogenomics resolves the timing and pattern of insect evolution. *Science* **346**: 763–767.

Molnar C. 2019. *Interpretable machine learning: a guide for making black box models explainable*. [WWW document] URL https://christophm.github.io/interpretable-ml-book/ [accessed 27 May 2020].

Nagano AJ, Kawagoe T, Sugisaka J, Honjo MN, Iwayama K, Kudoh H. 2019. Annual transcriptome dynamics in natural environments reveals plant seasonal adaptation. *Nature Taxa* **5**: 74–83.

Park DS, Breckheimer I, Williams AC, Law E, Ellison AM, Davis CC. 2018. Herbarium specimens reveal substantial and unexpected variation in phenological sensitivity across the eastern United States. *Philosophical Transactions of the Royal Society of London. Series B: Biological Sciences* **374**: 20170394.

Parmesan C. 2006. Ecological and evolutionary responses to recent climate change. *Annual Review of Ecology, Evolution, and Systematics* **37**: 637–669.

Pedregosa F, Varoquaux G, Gramfort A, Michel V, Thirion B, Grisel O, Blondel M, Prettenhofer P, Weiss R, Dubourg V *et al.* 2011. Scikit-learn: machine learning in Python. *Journal of Machine Learning Research* **12**: 2825–2830.

Renner SS, Zohner CM. 2018. Climate change and phenological mismatch in trophic interactions among plants, insects, and vertebrates. *Annual Review of Ecology, Evolution, and Systematics* **49**: 165–182.

Schwartz MD, Ahas R, Aasa A. 2006. Onset of spring starting earlier across the Northern Hemisphere. *Global Change Biology* **12**: 343–351.

Sen PK. 1968. Estimates of the regression coefficient based on Kendall's tau. *Journal of American Statistical Association* **63**: 1379–1389.

Singer FM. 2018. *Blossoms. And the genes that make them*. Oxford, UK: Oxford University Press.

Sparks TH, Menzel A. 2002. Observed changes in seasons: an overview. *International Journal of Climatology* **22**: 1715–1725.

Templ B, Templ M, Filzmoser P, Lehoczky A, Bakšienė E, Fleck S, Gregow H, Hodzic S, Kalvane G, Kubin E *et al.* 2017. Phenological patterns of flowering across biogeographical regions of Europe. *International Journal of Biometeorology* **61**: 1347–1358.

Tooke F, Battey NH. 2010. Temperate flowering phenology. *Journal of Experimental Botany* **61**: 2853–2862.

Tropp JA, Gilbert AC. 2007. Signal recovery from random measurements via orthogonal matching pursuit. *IEEE Transactions on Information Theory* **53**: 4655–4666.

Tropp JA, Gilbert AC, Strauss MJ. 2006. Algorithms for simultaneous sparse approximation. Part I: greedy pursuit. *Signal Processing* **86**: 572–588.

Uppala SM, KÅllberg PW, Simmons AJ, Andrae U, Bechtold VDC, Fiorino M, Gibson JK, Haseler J, Hernandez A, Kelly GA *et al.* 2005. The ERA-40 re-analysis. *Quarterly Journal of the Royal Meteorological Society* **131**: 2961–3012.

Wadgymar SM, Ogilvie JE, Inouye DW, Weis AE, Anderson JT. 2018. Phenological responses to multiple environmental drivers under climate change: insights from a long-term observational study and a manipulative field experiment. *New Phytologist* **218**: 517–529.

Walther GR, Post E, Convey P, Menzel A, Parmesan C, Beebee TJC, Fromentin JM, Hoegh-Guldberg O, Bairlein F. 2002. Ecological responses to recent climate change. *Nature* **416**: 389–395.

Wang Y, Zhao H, Wang Y, Yu S, Zheng Y, Wang W, Chan Z. 2019. Comparative physiological and metabolomic analyses reveal natural variations of tulip in response to storage temperatures. *Planta* **249**: 1379–1390.

White LM. 1979. Relationship between meteorological measurements and flowering of index species to flowering of 53 plant species. *Agricultural Meteorology* **20**: 189–204.

Zhao C, Hwang WL, Lin CL, Chen W. 2018. Greedy orthogonal matching pursuit for subspace clustering to improve graph connectivity. *Information Science* **459**: 135–148.

Zheng BY, Chenu K, Dreccer MF, Chapman SC. 2012. Breeding for the future: what are the potential impacts of future frost and heat events on sowing and flowering time requirements for Australian bread wheat (*Triticum aestivium*) varieties? *Global Change Biology* **18**: 2899–2914.

Supporting Information

Additional Supporting Information may be found online in the Supporting Information section at the end of the article.

Fig. S1 A 33 yr' time series of the 16 meteorological parameters.

Fig. S2 Geographic setting of the test area.

Fig. S3 Climatological daily mean values of atmospheric variables determined for the period of 1 January 1958–31 December 2000.

Fig. S4 Normalized histograms for daily deviations of atmospheric variables from the spatial mean value (see Fig. S2).

Fig. S5 Graphical representation of the cross-correlation matrix for the 16 meteorological variables.

Fig. S6 Time dependent cross correlations $X(\tau)$ for representative parameters.

Fig. S7 A 10 yrs' time series of the 16 daily mean meteorological parameter anomalies.

Fig. S8 A 33 yrs' time series of the 16 monthly mean meteorological parameter anomalies.

Fig. S9 The result of shuffling test of the OMP regression procedure.

Fig. S10 Linear tendencies of flowering dates.

Fig. S11 Summary plot for linear tendencies of flowering dates.

Fig. S12 Explained variance R^2 of flowering date fluctuation fits for each taxon.

Fig. S13 Summary statistics for nonzero OMP coefficients, when snow depth is excluded from the input parameter set.

Fig. S14 Illustration of the OMP regression with two daily snow depth anomalies for taxon index 44 (*Puschkinia scilloides*).

Fig. S15 The same as Fig. S14, regression for taxon index 44 with direct snow depth values.

Fig. S16 Illustration of the OMP regression with two daily snow depth anomalies for taxon index 313 (*Colchicum autumnale*).

Fig. S17 The same as Fig. S16, regression for taxon index 313 with direct snow depth values.

Fig. S18 Illustration of the OMP regression with two daily snow depth anomalies for taxon index 207 (*Tulipa gesneriana*).

Fig. S19 The same as Fig. S18, regression for taxon index 207 with a single snow depth anomaly.

Fig. S20 The same as Fig. S19, regression for taxon index 199 (*Ornithogalum lanceolatum*).

Table S1 List of taxa, abundancy index, mean flowering day of year in the period of 1968–2001, tendency of flowering time (fitted linear slope is in units of days/decade), and standard error of the fitted slope.

Please note: Wiley Blackwell are not responsible for the content or functionality of any Supporting Information supplied by the authors. Any queries (other than missing material) should be directed to the *New Phytologist* Central Office.

See also the Commentary on this article by Wesselingh, **228**: 1458–1459.